Recent development in the LIGO Input Optics

Sanichiro YOSHIDA, Guido MUELLER, Thomas DELKER, Qi-ze SHU, David REITZE, D. B.TANNER
Department of Physics, University of Florida, Gainesville, FL 32611-8440, USA
Jordan CAMP, Jay HEEFNER, Bill KELLS, Nergis MAVALVALA, Dale. OUIMETTE, Haisheng RONG
California Institute of Technology, Pasadena, CA 91125, USA
Rana ADHIKARI, Peter FRITSCHEL, Mike ZUCKER
Massachusetts Institute of Technology, Cambridge, MA 02139, USA
Daniel SIGG
LIGO Hanford Observatory, Richland, WA 99352-1970, USA

Abstract

We present recent results on high sensitivity measurements of modal distortions in LIGO Input Optics components. We also demonstrate a high-sensitivity method to characterize and improve the mode matching into optical cavities based on heterodyne detection of cylindrical transverse cavity modes.

1. Introduction

The LIGO Input Optics (IO) is the interface between the pre-stabilized laser (PSL) and the LIGO interferometer. The IO conditions the laser light so that its properties are compatible with the primary scientific requirements for the LIGO and serves four primary functions:

- RF modulation - the laser light must have sidebands used for both length and alignment sensing and control. The IO uses electro-optic phase modulators (EOMs) to generate sidebands.
- Mode stabilization - the laser light must be frequency and spatially stabilized before it can be used to provide length and alignment sensing for the interferometer. A mode cleaner provides frequency and spatial stabilization to the laser light.

- The light must be delivered to the interferometer with a proper Gaussian mode so that it will efficiently couple into the interferometer cavities. The IO provides for the mode matching of the light between the mode cleaner and the interferometer and for the measurement of mode mismatch.
- Back-reflected light from the interferometer is used for interferometer alignment control. The IO provides diagnostic signals using a Faraday isolator. This also prevents light from coupling back into the laser and introducing excess phase noise.

In these Proceedings, we report on some of the recent developments of the LIGO Input Optics. We specifically focus on i) measurements of wavefront distortions in the Input Optics components and ii) mode matching diagnostics for the LIGO interferometers.

2. Input Optics overview

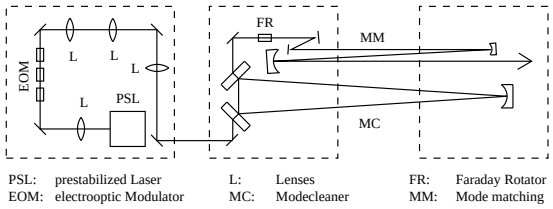

Fig. 1. input optics layout

Fig.1 illustrates the conceptual IO optical layout for the 2 km interferometer. (The IO for the 4 km interferometers are similar in design.) The output beam from the PSL (8.5 W in TEM_{00}) is first introduced into a chain of EOMs for sideband generation. The EOM chain consists of three $LiNbO_3$ based EOMs with modulation frequencies at 68.8 MHz, 26.7 MHz, and 29.4 MHz. These sidebands are used for interferometer alignment sensing, interferometer length sensing, and mode cleaner length and alignment sensing, respectively. The output beam from the EOM chain is mode-matched into the mode cleaner by three mode-matching lenses and directed into the vacuum system by a step-up periscope (not shown in Fig. 1.). The mode cleaner is a suspended triangular resonator with a nominal finesse of 1550 which provides active frequency noise suppression through feedback to the PSL, passive frequency noise suppression above its cavity pole frequency (4 KHz), and passive spatial stabilization at all frequencies. The output from the MC enters a Faraday isolator (FI) for isolation and diagnostic beam delivery The beam passing through the FI is then delivered to the mode-matching telescope

(MMT) for mode-matching to the core optics. The mode-matching telescope consists of three suspended concave mirrors which can be adjusted in position to provide optimal coupling of TEM_{00} mode into the interferometer. The mode-matching characterization diagnosis is performed by a heterodyne technique using a circularly-segmented photo-detectors called the Bullseye detector, described in more detail below. Two Bullseye detectors are placed at the bright port of the FI.

3. Thermal wavefront distortion

When the PSL beam passes through transmissive optics, its wavefront is distorted by the thermal lens generated by virtue of its high average power. The resultant modal distortion can compromise the coupling of light into the interferometer. We have investigated this effect by measuring the change in the optical path length with a Shack-Hartmann wavefront detector [6]. The detailed description of these experiments is described in [8]. Briefly, a well characterized probe laser (TEM_{00} Helium Neon laser beam) was transmitted through the optic under study collinearly with the 1.06 μm beam and then measured using the Shack Hartmann detector. The optical path length change (ΔOPL) in the probe beam due to thermal lensing was then calculated with respect to the beam center.

3.1. EOMs

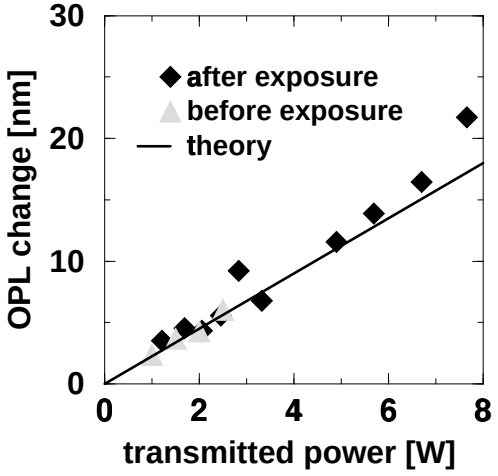

Fig. 2. Thermal lens in EOM

The propagation of high average power laser radiation in the EOMs has two potentially deleterious consequences. First, it can change the distort the mode of the PSL beam such that the mode matching lenses cannot correct it

Table 1. Numbers used to calculate ΔOPL

$material$	$\gamma(1/cm)$	$dn/dT(1/k)$	$\alpha(1/K)$	n	$l(cm)$	$\kappa(W/m\,K)$
$LiNbO_3$	6.25×10^{-4}	3.8×10^{-5}	$4.0 \times 10_{-6}$	2.156	4	5.6
TGG	1.5×10^{-3}	2.0×10^{-5}	$9.4 \times 10_{-6}$	1.95	2	7.4

for the required level of mode matching to the MC. In addition, the $LiNbO_3$ crystal can suffer permanent photo-refractive damage due to sustained exposure. To determine the severity of these effects, the EOMs were exposed to 10 W continuous wave Nd:YAG radiation for 600 hours. Fig. 2. shows the measured thermal lens before and after the 600 hour exposure, along with a theoretical value based on the following equation [4].

$$\Delta OPL = 0.07741\ P\ l\frac{\gamma}{\kappa}(\frac{dn}{dT} + \alpha n)[(\frac{r}{w})^2 + 0.4\,(\frac{r}{w})] \qquad (1)$$

where γ is the absorption coefficient, l is the crystal length, κ is the thermal conductivity, dn/dT is the temperature coefficient of the refractive index, α is the thermal expansion coefficient, r is the radius and w is the spot size of the Nd:YAG laser. Table 1. lists the parameters used for eq. 1. The constant 0.07741 appearing at the beginning of eq. 1 is comes from the expression of temperature rise caused by a Gaussian beam in a cylindrical substrate [7].

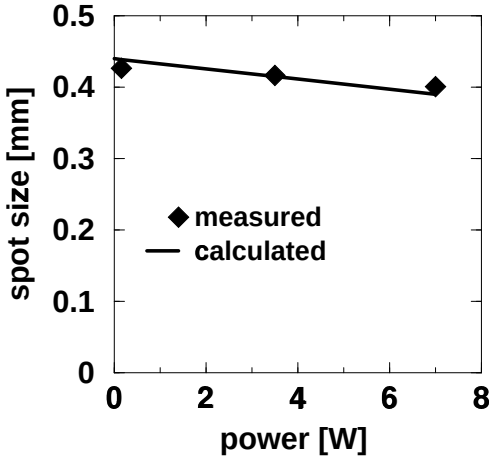

Fig. 3. Power dependence of PSL spot size after EOM chain

Fig. 2. shows the same slope before and after the 600-hour exposure, indicating that there was no permanent photorefractive damage in the crystal. This slope agrees with the theoretical value of 2.2 nm/W calculated at the spot size of the 1.06 μm beam.

From Fig. 2., ΔOPL at the spot size for the designed PSL power of 8.5 W can be estimated to be 18.7 nm. Since the spot size of the PSL beam in the EOM is 0.4 mm, the effective focal length of this thermal lens f_{EOM} is estimated to be 4.2 m for one EOM.

$$f_{EOM} = \frac{w^2}{2\,\Delta OPL} \tag{2}$$

Thus, the total effective focal length for the three EOMs can be estimated in the order of 1 m. This changes the waist size of the PSL beam from 0.39 mm to 0.38 mm and shifts the waist location by 1.8 mm. This change is well within the range correctable by the mode matching lenses.

To confirm the measurement by the Shack-Hartmann wavefront detector, we measured the actual beam size using a beam scanner. This measurement was made in-situ using the PSL beam and the EOM chain. Fig. 3. compares the beam size at 29 cm from the EOM with the theoretical curve that we obtained using the effective focal length f_{EOM} and the ray matrix representing a thin lens. Assuming that the three EOMs have the same effective focal length and neglecting the propagation distance between them, a simple ray matrix can be used to compute the propagation parameter. From the slope of Fig.2., ΔOPL can be written as a function of laser power P as,

$$\Delta OPL = a\,P \tag{3}$$

where $a = 2.2 \times 10^{-9} m/W$. Substituting eqs. 2 and 3 into the ray matrix, we obtained the theoretical curve in Fig. 3.. The measured and calculated spot sizes show a reasonable agreement.

3.2. Faraday isolator

We also measured the thermal lens in the terbium gallium garnet crystal in the Faraday isolator (FI) using the same method as the EOM. Because the FI is positioned behind the mode cleaner, any changes in mode parameters directly affects the coupling of light into the interferometer. In a separate measurement, we confirmed that the thermal lensing in the polarizers used in the FI is negligibly small. Thus, the measurement for the TGG crystal is sufficient to estimate the thermal lens. Fig. 4. shows ΔOPL at the spot size of the 1.06μm beam along with the theoretical value based on eq. 1. The numbers used for this calculation are listed in the Table 1. Good agreement is seen between the measurement and calculation.

Fig. 5. shows the effective focal length of the thermal lens in FI as a function of the laser power. At the power level of 8.5 W, the focal length is 90 m. This

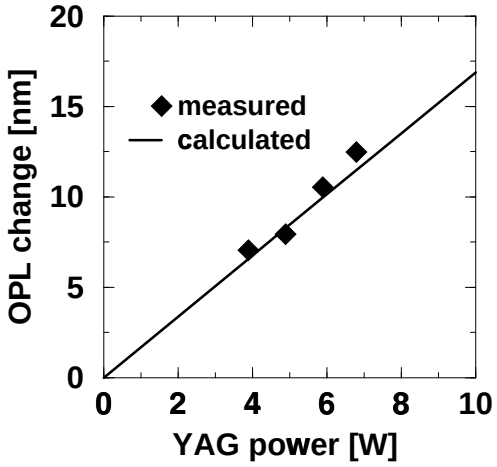

Fig. 4. Thermal lens in Faraday rotator

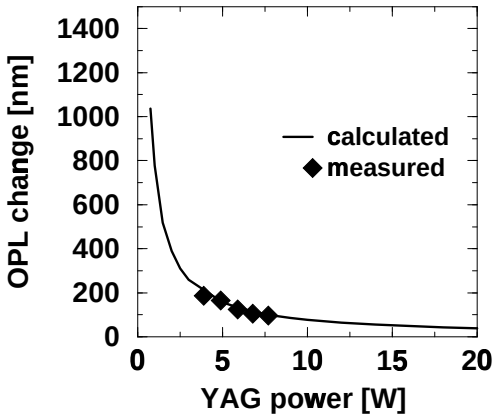

Fig. 5. Effective focal length of thermal lens in Faraday rotator

change in the beam curvature is easily corrected by adjusting the location of the optics forming the MMT.

4. Bullseye detector

In order to accurately diagnose the amount on higher order (cylindrical) mode mismatch caused by thermal distortions and improper telescope positioning in-situ, we have developed a heterodyne technique [5] capable of measuring the mode mismatch between a zeroth order Gaussian input beam and the fundamental eigenmode of a cavity. This technique utilizes the fact that for small mismatches, the zeroth order Gaussian mode ($\hat{U}_{00}$) of the input field can be expressed as a linear combination of the zeroth order (U_{00}) and first order (U_{10}) Laguerre Gauss

eigenmodes (or zeroth order and second order Hermite Gauss eigenmodes) of the cavity [1]:

$$\hat{U}_{00} = U_{00} + (b_1 + ib_2)U_{10} \qquad \text{with} \qquad b_1 = \frac{\delta w_0}{\hat{w}_0}, \quad b_2 = \frac{\delta z}{2\hat{z}_R} \tag{4}$$

where all modes are taken at the waist of the cavity.
The in-phase component of the amplitude of the first order Laguerre Gauss mode is proportional to the mismatch in waist size (δw_0), the quadrature component to the mismatch in waist position (δz). $\hat{w}_0$ and $\hat{z}_R$ are the waist size and the Rayleigh range of $\hat{U}_{00}$.

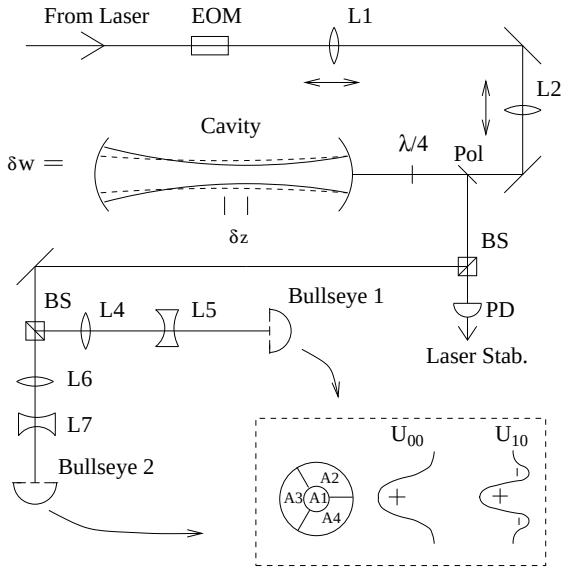

Fig. 6. Experimental setup for the Bullseye measurement

In the Pound Drever Hall technique [2], the zeroth order Gaussian mode of the light field is kept on resonance with the cavity using phase modulation spectroscopy followed by an active feedback loop. That technique measures the beat between the zeroth order Gaussian modes of the carrier and of the PM sidebands with a single area photo detector. Our technique measures the beat between the zeroth order Gaussian mode of the sidebands and the first order Laguerre Gauss mode of the carrier and vice versa with two different annular segmented photo detectors (Bullseyes, see inset of Fig. 6.). The technique is the analog of the alignment sensing and control system used in LIGO [3]The difference in the photocurrents between the outer segment A0 and the inner segment A1 has the following AC-component:

$$\Delta I_{ac} \;=\; sin(\Omega t)\Im\Big\{ r_{FP}\left[\int_{A0} |U_{00}(x,y)|^2 - \int_{A1} |U_{00}(x,y)|^2\right]$$

$$+ \quad (1 - r_{FP})(b_1 + ib_2) \left[\int_{A0} U_{00} U_{10}^*(x,y) - \int_{A1} U_{00} U_{10}^*(x,y) \right] \Big\} \qquad (5)$$

where Ω is the PM frequency, r_{FP} is the amplitude reflectivity of the cavity for the carrier in the zeroth order mode. The first order Laguerre Gauss mode of the carrier and all spatial modes of the sidebands are not resonant in the cavity.

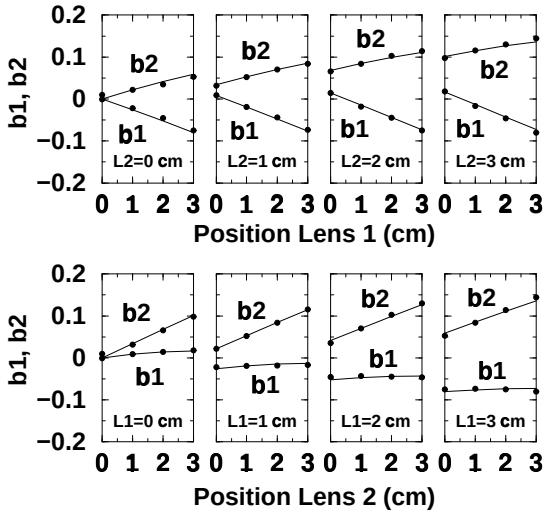

Fig. 7. Experimental and numerical results of Bullseye measurement

The areas A1 and A0 are of such a size that the integrals over the zeroth order modes are nominally equal. In addition, the PDH-feedback loop keeps $\Im(r_{FP}) \approx 0$. Therefore, the first half of equation (5) will only contribute in second order to this difference.

The difference of the second set of integrals is a complex number with an amplitude of the order of 0.33. Its phase is two times the Gouy-phase accumulated during the propagation from the waist of the cavity to the Bullseye detector.

The accumulated Gouy phase for each detector is set to 135 and 90 degrees, respectively such that the demodulated signal of the first arm is proportional to the in-phase component b_1 and of the second arm to the quadrature component b_2 of the amplitude of the first order Laguerre-Gauss mode.

A tabletop prototype has been used to validate these ideas. The experimental setup is shown in Fig. 6.. We measured the Bullseye signals for various combinations of lens positions. The results are compared in Fig. 7. with a numerical model based on Gaussian mode theory. The measured signals were fitted to the computed signals using only 1 fitting parameter for each detector.

Our results show that the smallest achieved amplitude of the first order Laguerre Gauss mode at lens positions 0 for both lenses is lower than 0.03 times the ampli-

tude of the fundamental transverse mode. This indicates that the mode matching is about 99.98% of the best possible value.

5. Acknowledgement

We are grateful for the advice and support by Stan Whitcomb and Rick Savage. This work is supported by the National Science Foundation through grants PHY92-10038 and PHY97-22114.

6. References

1. Anderson D.Z., Appl. Opt. 23, 2944 (1984)
2. Drever R.W.P., Hall J.L., Kowalski F.V., Hough J., Ford G.M., Munley A.J., Ward H., Appl. Phys. B 31, 97 (1983)
3. Hefetz Y., Mavalvala N., Sigg D., J. Opt. Soc. Am. B 14, 1597 (1997)
4. Mansell J., private communication (1997)
5. Mueller G., Shu Q., Adhikari R., Tanner D.B., Reitze D., Sigg D., Mavalvala N., Camp J., accepted at Optics Letters
6. Neal D. R., Armstrong D. J., Turner W. T., SPIE 2993, 1-10 (1997)
7. Strain K., Danzmann K., Mizuno J., Nelson P., Rüdiger A., Schilling R., Winkler W., Phys. Lett. A, 194, 124-132 (1994)
8. Yoshida S., Khazanov E., Kulagin O., Mansell J., Gorlenko A., Reitze D., Adhikari R., Delker T., Shu Q., Mueller G. and Tanner D., LIGO document T980021-00-D (1998)